9-1999

# Parity Violation in Neutron Resonances of 103Rh

D A. Smith
*Los Alamos National Laboratory*

J D. Bowman
*Los Alamos National Laboratory*

Bret E. Crawford
*Gettysburg College*

***See next page for additional authors***



Smith, D. A., Bowman, J. D., Crawford, B. E., Grossmann, C. A., Haseyama, T., Masaike, A., Matsuda, Y., Mitchell, G. E., Penttila, S. I., Roberson, N.R., Seestrom, S. J., Sharapov, E. I., Stephenson, S., & Yuan, V. W. (1999). Parity Violation in Neutron Resonances of 103Rh. Physical Review C, 60(045503). http://dx.doi.org/10.1103/PhysRevC.60.045503

# Parity Violation in Neutron Resonances of 103Rh

**Abstract**

Parity nonconservation (PNC) was studied in p-wave neutron resonances of $^{103}$Rh in the neutron energy range 30 to 490 eV. The helicity dependence of the neutron total cross section of rhodium was determined by capture measurements with the time-of-flight method at the Manuel Lujan Neutron Scattering Center at the Los Alamos National Laboratory. A total of 32 p-wave resonances were studied and statistically significant longitudinal asymmetries were observed for resonances at $E_n$=44.5, 110.8, 321.6, and 432.9 eV. A statistical analysis treating the PNC matrix elements as random variables yields a weak spreading width$\Gamma_w=(1.42_{-0.59}^{+1.21})\times10^{-7}$eV.

**Disciplines**

Atomic, Molecular and Optical Physics | Physics

**Authors**

D A. Smith, J D. Bowman, Bret E. Crawford, C A. Grossmann, T Haseyama, A Masaike, Y Matsuda, G E. Mitchell, S I. Penttila, N R. Roberson, S J. Seestrom, E I. Sharapov, Sharon L. Stephenson, and V W. Yuan

# Parity violation in neutron resonances of $^{103}$Rh

D. A. Smith,[1] J. D. Bowman,[1] B. E. Crawford,[2,*] C. A. Grossmann,[3] T. Haseyama,[4] A. Masaike,[4,†] Y. Matsuda,[4,‡] G. E. Mitchell,[3] S. I. Penttila,[1] N. R. Roberson,[2] S. J. Seestrom,[1] E. I. Sharapov,[5] S. L. Stephenson,[3,*] and V. W. Yuan[1]

[1]*Los Alamos National Laboratory, Los Alamos, New Mexico 87545*

[2]*Duke University, Durham, North Carolina 27708*
*and Triangle Universities Nuclear Laboratory, Durham, North Carolina 27708-0308*

[3]*North Carolina State University, Raleigh, North Carolina 27695-8202*
*and Triangle Universities Nuclear Laboratory, Durham, North Carolina 27708-0308*

[4]*Physics Department, Kyoto University, Kyoto 606-01, Japan*

[5]*Joint Institute for Nuclear Research, Ru-141980 Dubna, Russia*

(Received 7 April 1999; published 16 September 1999)

Parity nonconservation (PNC) was studied in $p$-wave neutron resonances of $^{103}$Rh in the neutron energy range 30 to 490 eV. The helicity dependence of the neutron total cross section of rhodium was determined by capture measurements with the time-of-flight method at the Manuel Lujan Neutron Scattering Center at the Los Alamos National Laboratory. A total of 32 $p$-wave resonances were studied and statistically significant longitudinal asymmetries were observed for resonances at $E_n = 44.5$, 110.8, 321.6, and 432.9 eV. A statistical analysis treating the PNC matrix elements as random variables yields a weak spreading width $\Gamma_w = (1.42^{+1.21}_{-0.59}) \times 10^{-7}$ eV. [S0556-2813(99)06810-7]

PACS number(s): 25.40.Ny, 11.30.Er, 27.90.+b

## I. INTRODUCTION

The usual approach to parity nonconservation (PNC) in light nuclei involves parity doublets (closely spaced states of the same angular momentum and parity) and the measurement of a parity-forbidden observable [1]. The major difficulty in this approach is calculating the wave functions of the initial and final states with sufficient precision. The observation of very large parity violation in neutron resonances in heavy nuclei [2] led to a new approach. The compound nucleus is now considered to be a unique laboratory for studies of fundamental symmetries [3–5]. For some $p$-wave resonances the helicity dependence of the neutron total cross section shows very large asymmetries. These large asymmetries are produced by the mixing of neighboring $s$-wave resonances with the $p$-wave resonances, as first predicted by Sushkov and Flambaum [6]. In the initial observations of PNC effects in heavy nuclei only the lowest energy neutron resonances were observed. In the new analysis approach, the compound nucleus is considered a statistical system and the symmetry breaking matrix elements are taken to be random variables. Since the analysis is statistical, the observation of a number of PNC effects is essential.

The TRIPLE Collaboration was formed to measure many asymmetries in a given nuclide. The first measurements were performed on $^{238}$U and $^{232}$Th [7,8] and then repeated with an improved experimental system [9,10]. Many PNC effects were observed and the rms weak mixing matrix elements were determined for these nuclei. One key question is whether the effective nucleon-nucleus weak interaction is mass dependent. The nuclei initially measured are at the peak of the $4p$ neutron strength function. The next most reasonable mass region to study is near the peak of the $3p$ neutron strength function at $A \approx 100$. For even-mass targets in this region the level densities are much lower than for uranium or thorium. Odd-mass targets have higher level densities compared with even-mass targets in the same region. Therefore most of the PNC measurements that our group has performed in the $A \approx 100$ mass region are with odd-mass targets. Odd-mass nuclei that have been measured include $^{93}$Nb [11], $^{107,109}$Ag [12], $^{113}$Cd [13], $^{117}$Sn [14], $^{121,123}$Sb and $^{127}$I [15], and $^{133}$Cs [16]. The nuclide $^{103}$Rh was considered an excellent candidate for study of PNC effects, since rhodium is monoisotopic and is located near the peak of the $3p$ neutron strength function. PNC effects were observed for almost all of the nuclides studied, including rhodium. However, the price that is paid for the study of odd-mass targets is an increased complication in the analysis. The spectroscopic information is very important (especially the spins of the $s$- and $p$-wave resonances). Absent this information the analysis must average over various possibilities, which results in larger uncertainties for the value of the rms weak matrix element and the weak spreading width. The neutron resonance spectroscopy has been remeasured for rhodium by our group [17], but information is still missing for most of the resonance spins. The effect of these complications is discussed in the text below.

In Sec. II the experimental procedure is described. In Sec. III the analysis to obtain the resonance parameters and the PNC longitudinal asymmetries is discussed and the experimental results presented. The analysis to determine the weak spreading width is described in Sec. IV. In Sec. V the weak spreading width determined for $^{103}$Rh is compared with the other spreading widths obtained by the TRIPLE Collaboration. A brief summary is given in Sec. VI.

*Present address: Gettysburg College, Gettysburg, PA 17325.

†Present address: Fukui University of Technology, 3-6-1 Gakuen Fukui-shi, Japan.

‡Present address: Institute of Physical and Chemical Research (RIKEN), Saitama 351-0198, Japan.

 

## II. EXPERIMENTAL PROCEDURE

At the Manuel Lujan Neutron Scattering Center (MLNSC), neutrons are created by the spallation process. The 800-MeV proton beam from the Los Alamos Neutron Science Center (LANSCE) linac is chopped, injected into the Proton Storage Ring (PSR), accumulated and there directed towards a tungsten spallation target. The neutrons resulting from this proton pulse are moderated in a water moderator and collimated [18]. The data were measured at flight path 2 of MLNSC. The neutron energy was determined from the time-of-flight over a 59.4-m distance from source to detector. The detector [19,20] is an array of 24 CsI crystals with approximately $3.0\pi$ of detection solid angle. The crystals are packed tightly around the target in two arrays of 12 crystals each, with a 20-cm cylindrical hole through the middle to allow access for the neutron beam. The scintillation light from the CsI crystals is detected by photomultiplier tubes whose signals are converted to logic pulses by constant fraction discriminators. In order to reduce the rate of the background signal, a coincidence of two signals from the detector was required for an event to be recorded. The event pulses were counted by a multiscaler attached to an averaging memory. The start time of the multiscaler spectra is derived from the proton pulse. The multiscaler dwell time was set to 100 ns to cover a time-of-flight range of 0 to 0.8192 ms. This corresponds to neutron energies from about 30 eV to 2 keV. The detector shielding and electronics are described in detail by Seestrom *et al.* [20].

The relative neutron flux for each proton pulse was monitored by a pair of ionization chambers [21]. This neutron monitor signal is important for these asymmetry measurements, since large changes in neutron flux between two proton pulses can produce a false asymmetry.

The neutron beam was polarized by transmission through a polarized proton filter. The polarized protons were produced by dynamic polarization of frozen ammonia [22,23]. The ammonia was cooled in liquid $^4$He to 1 K at the center of a 5-T split-coil superconducting magnet. The proton polarization direction could be reversed by changing the microwave frequency. This is a convenient way to test for systematic errors. Since this change took several hours, the proton polarization direction was changed only once during the rhodium experiment. The neutron polarization is changed on a short time scale by a system of longitudinal and transverse magnetic fields [24]—a neutron spin flipper. The longitudinal fields are parallel to the beam momentum for the first half of the spin flipper and antiparallel for the second half. The combination of the transverse and longitudinal fields produces a net magnetic field which is constant in magnitude and whose direction rotates 180° over the length of the spin flipper. The neutron spin follows the net magnetic field and its polarization is reversed. With no transverse field the polarization state is unchanged. Each spin flipper state lasted 10 seconds. To reduce the effects of gain drifts and residual magnetic fields, the spin state was changed according to an eight step sequence. The sequence used was $0++0-00-$, where 0 is spin parallel to the beam direction (no transverse field), and $\pm$ is spin antiparallel to beam direction (transverse field in the up or down direction). Each eight-step sequence was labeled good or bad depending on whether the neutron beam monitor varied more than 8% in intensity over the course of the sequence. At the end of each half-hour the accumulated spectra were saved as a run.

The polarization of the neutron beam was maintained during the passage of the beam from the proton polarizer to the interaction target by use of a magnetic field in the beam pipe. For low energy neutrons and the long distance of 59 m, the earth's magnetic field can produce significant depolarization. The entire length of the beam pipe from the end of the spin flipper to the target was wrapped in coils of wire and a constant electric current applied [25]. The beam polarization at the target was determined by comparing a transmission measurement on $^{139}$La to the PNC asymmetry in the 0.74-eV resonance in $^{139}$La. The asymmetry value of $9.35\pm0.35\%$ for this resonance has been very well determined in previous measurements [26]. The polarization was monitored by measurement with a $^6$Li detector of the neutron transmission through a sample of lanthanum metal placed behind the interaction target. For each run an approximate value of the asymmetry in the 0.74-eV resonance was obtained in order to monitor the polarization of the neutron beam at the target.

The target was assembled from plates of rhodium metal (99.9% pure) in the form of a 10-cm diameter disk of areal density 2.99 g/m$^2$.

## III. DATA ANALYSIS

The first step in the data analysis was to sort the data into acceptable and unacceptable runs. A data run was labeled unacceptable if the asymmetry of the entire time-of-flight spectrum was greater than 0.06%. The acceptable spectra were summed to obtain the experimental time-of-flight spectrum for each spin state. In the final summed spectra, there was a 0.003% asymmetry between time-of-flight spectra for each spin state.

The summed spectra for each spin state were analyzed with a fitting code FITXS developed specifically for the TRIPLE experiments [27]. FITXS minimizes $\chi^2$ for a region of the time-of-flight spectrum to determine such parameters as the resonance energy, neutron width, radiative width, beam length, neutron flux, and others. The neutron resonance parameters were then held fixed while the longitudinal asymmetries were determined. The details of the neutron spectroscopy analysis and the resulting neutron resonance parameters of $^{103}$Rh are given in Ref. [17].

The yield asymmetries were then obtained from the difference in neutron cross section between the two neutron spin states for each $p$-wave resonance $\mu$:

$$p_\mu(E)=\frac{\sigma_\mu^+(E)-\sigma_\mu^-(E)}{\sigma_\mu^+(E)+\sigma_\mu^-(E)}. \tag{1}$$

The yield asymmetries were then corrected for the beam polarization (a typical beam polarization was about 70%). There was also a correction applied for the spin-flipper efficiency. This small correction was constant over the energy range of this experiment. There was also a correction for the

TABLE I. Longitudinal asymmetries $p$ and enhancement factors $A_J$ for $p$-wave resonances in $^{103}$Rh. The $A_J$ values are calculated assuming that the resonance has $J=0$ or 1. No significant asymmetries were observed above 490 eV.

| Energy (eV) | $A_0$ (1/eV) | $A_1$ (1/eV) | $p$ (%) | $p/\delta p$ |
|---|---|---|---|---|
| 34.46 | 0.76 | 1.51 | 0.007±0.05 | 0.1 |
| 44.47 | 1.79 | 10.11 | 2.33±0.19 | 12.3 |
| 51.92 | 3.59 | 9.89 | −1.11±0.63 | 1.8 |
| 83.51 | 1.96 | 3.16 | −0.08±0.18 | 0.4 |
| 98.77 | 0.94 | 3.57 | 0.120±0.074 | 1.6 |
| 108.78 | 2.96 | 3.89 | −0.23±0.25 | 0.9 |
| 110.80 | 0.84 | 1.09 | 0.17±0.05 | 3.7 |
| 112.62 | 3.42 | 4.52 | 0.46±0.31 | 1.5 |
| 113.99 | 1.10 | 1.50 | 0.05±0.06 | 0.8 |
| 179.32 | 1.68 | 4.05 | 0.07±0.083 | 0.8 |
| 199.69 | 1.64 | 4.71 | 0.04±0.21 | 0.2 |
| 205.01 | 1.10 | 2.66 | 0.03±0.14 | 0.2 |
| 251.13 | 0.60 | 14.50 | −0.45±0.32 | 1.4 |
| 263.12 | 0.16 | 2.10 | −0.06±0.05 | 1.1 |
| 264.21 | 0.24 | 3.40 | −0.002±0.09 | 0.0 |
| 312.46 | 0.33 | 6.82 | 0.26±0.19 | 1.3 |
| 321.63 | 0.12 | 10.10 | 0.36±0.12 | 3.1 |
| 327.75 | 0.18 | 3.61 | −0.27±0.12 | 2.3 |
| 353.89 | 0.36 | 2.44 | −0.46±0.31 | 1.5 |
| 362.49 | 0.17 | 1.10 | −0.11±0.12 | 0.9 |
| 366.30 | 0.07 | 0.47 | −0.03±0.05 | 0.6 |
| 373.93 | 0.14 | 0.88 | −0.02±0.10 | 0.2 |
| 376.31 | 0.26 | 1.73 | 0.03±0.27 | 0.1 |
| 388.62 | 0.18 | 1.49 | −0.11±0.15 | 0.7 |
| 427.59 | 0.27 | 9.78 | −0.43±0.51 | 0.8 |
| 432.91 | 0.08 | 8.78 | −0.45±0.16 | 2.9 |
| 443.93 | 0.17 | 6.44 | 0.29±0.32 | 0.9 |
| 447.06 | 0.21 | 6.46 | −1.10±0.47 | 2.3 |
| 472.83 | 0.08 | 0.76 | −0.10±0.08 | 1.3 |
| 479.15 | 0.33 | 2.86 | 1.16±0.77 | 1.5 |
| 486.44 | 0.07 | 0.60 | 0.01±0.08 | 0.1 |
| 489.23 | 0.20 | 1.54 | 0.06±0.46 | 0.1 |

energy dependence of the depolarization in the beam pipe. The absolute polarization was determined just after the reaction target by the $^{139}$La transmission measurement. However, the efficiency of the polarization transfer over the length of the beam pipe was slightly energy dependent [28]. These corrections were applied to the yield asymmetries to obtain the final parity violation asymmetries of the $p$-wave resonances.

Although all resonances up to 2 keV were analyzed, no significant parity violation asymmetries were observed above 500 eV—these null results are not listed here. As a check of the experimental systematics, many $s$-wave resonances were analyzed, and no significant asymmetries were observed for these resonances. In Table I, the measured asymmetries are listed for the $p$-wave resonances. There are four resonances with significant asymmetries (statistical significance 2.5 $\sigma$ or greater). To illustrate the sensitivity of the experiment, a null result is shown in Fig. 1. The sum and difference of the yields for the two neutron spin states are shown for the 34.4-eV $p$-wave resonance. The sum shows the resonance and the fit produced from the FITXS code. In the difference spectrum there is no obvious systematic dependence. In this experiment we believe the systematic errors to be less than $10^{-5}$, well below the measured statistical errors of about $10^{-3}$.

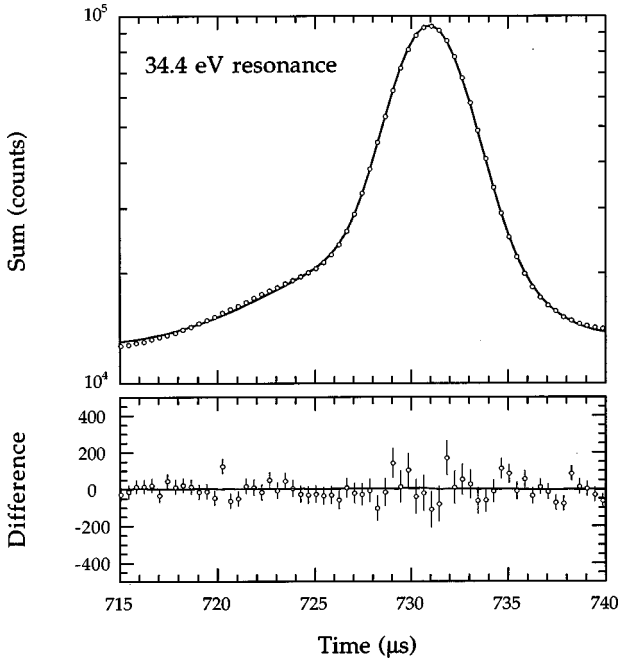


FIG. 1. Sum and difference data, between the two neutron spin states plotted as counts, in the region of the 34.4-eV resonance. The solid lines are fits to the data. This resonance displays no asymmetry, but illustrates the magnitude of the systematic errors of the system.

Two resonances with significant asymmetries are shown in Figs. 2 and 3. In Fig. 2 the sum and difference spectra are shown for the 44.5-eV resonance. In the sum spectrum the resonance can be seen along with the fit to the data. The sharp rise in count rate at the low time-of-flight end of the spectrum is due to the tail of the 46.8-eV $s$-wave resonance. The difference spectrum shows a large asymmetry for this resonance. For this case the difference spectrum displays a well-isolated resonance line shape that falls to zero on both sides of the resonance, although the count rate increases due to the tail of the nearby $s$-wave resonance. In Fig. 3 sum and difference spectra are shown in the region of the 110.8-eV resonance. This figure illustrates a common difficulty—in this small region there are four overlapping $p$-wave resonances. The multilevel fit to the data is shown in the sum spectrum. The difference spectrum shows a typical result, with only one resonance of the several $p$-wave resonances showing parity violation.

## IV. DETERMINATION OF WEAK SPREADING WIDTH

Once the asymmetries are obtained, a statistical analysis is performed to determine the rms weak mixing matrix element and the weak spreading width. The mixing between the

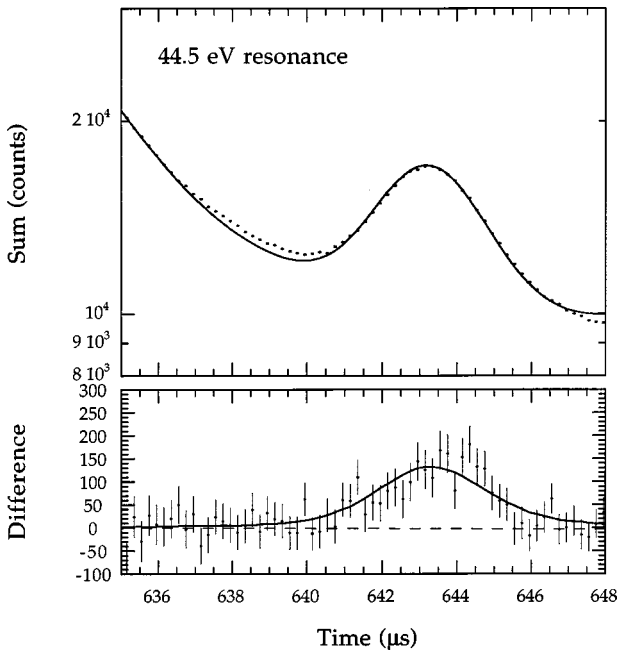


FIG. 2. Sum and difference data, between the two neutron spin states plotted as counts, in the region of the 44.5-eV resonance. The solid lines are fits to the data. The difference spectrum displays a highly significant asymmetry.

*s*- and *p*-wave resonances occurs only for resonances with the same $J$ value. For $^{103}$Rh, with target spin $I=1/2$, this complicates matters. There are two sets of *s*-wave resonances, $J=0$ and 1, and three sets of *p*-wave resonances, $J=0$, 1, and 2. In $^{103}$Rh the $J$ values for most of the *s*-wave resonances are known, but none for the *p*-wave resonances.

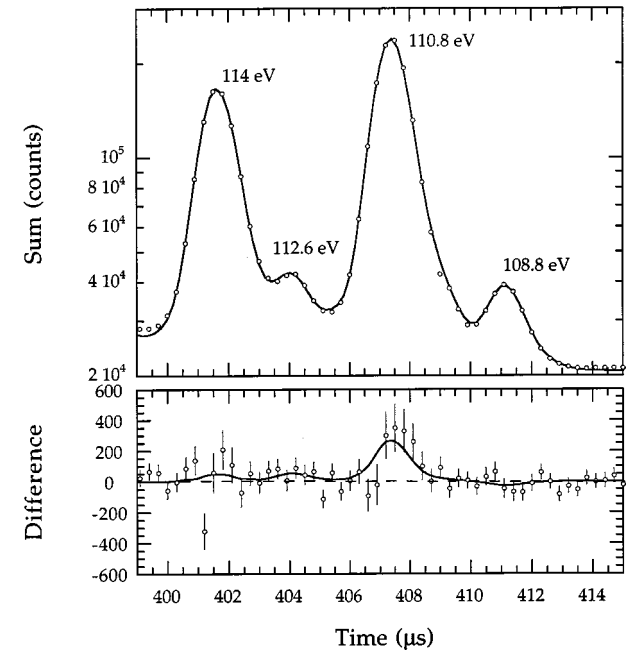


FIG. 3. Sum and difference data, between the two neutron spin states plotted as counts, in the region of the 110.8-eV resonance. The solid lines are fits to the data.

For this case the magnitude of the parity violating asymmetry for a given *p*-wave resonance $\mu$ is given by [29]

$$p_\mu = \sum_{\nu: J_\nu = J_\mu} \frac{2V_{\nu\mu}}{E_\mu - E_\nu} \frac{\sqrt{\Gamma_{\nu_n}}}{\sqrt{\Gamma_{\mu_n}}} \frac{g_{\mu_{1/2}}}{\sqrt{g^2_{\mu_{1/2}} + g^2_{\mu_{3/2}}}}, \tag{2}$$

where the summation is over all *s*-wave resonances $\nu$ with $J_\nu = J_\mu$, $V_{\nu\mu}$ is the weak interaction matrix element, $E_\nu$ and $E_\mu$ are the energies of the *s*- and *p*-wave resonances, $\Gamma_{\mu_n}$ and $\Gamma_{\nu_n}$ are the corresponding neutron widths, and $g_{\mu_{1/2}}$ and $g_{\mu_{3/2}}$ are the projectile-spin neutron amplitudes ($g^2_{\mu_{1/2}} + g^2_{\mu_{3/2}} = \sqrt{\Gamma_{\mu_n}}$). The neutron widths and resonance energies are known from our earlier measurement [17], and the weak interaction matrix element $V_{\nu\mu}$ is assumed to be a Gaussian random variable with variance $M^2$. The probability density function for the asymmetry can then be written:

$$P_p(p|MAR) = G(p, M^2A^2R^2). \tag{3}$$

The function $G$ is a mean-zero Gaussian distribution of the variable $p$ with a variance $M^2A^2R^2$, where $A$ and $R$ are

$$A^2_\mu = \sum_{\nu: J_\nu = J_\mu} \left(\frac{2}{E_\mu - E_\nu}\right)^2 \frac{\Gamma_{\nu_n}}{\Gamma_{\mu_n}} \quad \text{and} \quad R = \frac{g_{\mu_{1/2}}}{\sqrt{g^2_{\mu_{1/2}} + g^2_{\mu_{3/2}}}}. \tag{4}$$

The so-called enhancement factors $A = \sqrt{A^2_\mu}$ are determined from the resonance parameters. The amplitudes $g_{\mu_{1/2}}$ and $g_{\mu_{3/2}}$ are unknown, but are assumed to be Gaussian random variables. We define $X^2$ as the variance of $g_{1/2}$, and $Y^2$ the variance of $g_{3/2}$. The probability density functions of these quantities are Gaussian distributions:

$$P(g_{1/2}) = G(g_{1/2}, X^2) \quad \text{and} \quad P(g_{3/2}) = G(g_{3/2}, Y^2), \tag{5}$$

where $X^2$ and $Y^2$ can be related to the $S^1_{1/2}$ and $S^1_{3/2}$ *p*-wave strength functions. It is convenient to convert to polar coordinates: $g_{1/2} = r \sin\theta$, $g_{3/2} = r\cos\theta$, and $R = \sin\theta$. After integration over $r$ the probability density function becomes

$$P(\theta) = \frac{1}{2\pi} \frac{a}{a^2 \sin^2\theta + \cos^2\theta}, \tag{6}$$

where $a^2 = Y^2/X^2$ is the ratio of the $p_{3/2}$ to $p_{1/2}$ strength functions. This ratio has been measured in previous experiments for this nucleus; the value used in this analysis is $a^2 = 0.373 \pm 0.069$ [30]. The final probability density function for the measured asymmetries is

$$P_p(p|MA, a, \sigma) = \frac{2}{\pi} \int_0^{\pi/2} \frac{a}{a^2 \sin^2\theta + \cos^2\theta} \times G(p, M^2A^2 \sin^2\theta + \sigma^2) d\theta, \tag{7}$$

where $p$ and $\sigma$ are the magnitude and experimental error of the PNC longitudinal asymmetry.

The asymmetries and their errors were measured in the present experiment, the neutron widths and resonance energies were determined in our previous analysis [17], and the ratio $a$ is known from a previous experiment [30]. The $J$ values of the $p$-wave resonances are unknown and one does not know which $s$-wave resonances mix to cause parity violation. Since there are three sets of $p$-wave resonances, one can calculate the probability density function for the $p$-wave resonance assuming each of the three possible spin states. These three probability density functions can be then combined to determine the likelihood function. Since there are two sets of $s$-wave resonances with which to mix, there are in principle two different rms weak mixing matrix elements for rhodium, one for $J=0$ and one for $J=1$. We assume that these two matrix elements differ in strength only because of the $J$ dependence of the $s$-wave level density. This difference can be accounted for by defining the weak spreading width [3]:

$$\Gamma_w = \frac{2\pi M_J^2}{D_0(J)}, \tag{8}$$

where $M_J$ is the weak mixing matrix element for angular momentum $J$, and $D_0(J)$ is the average $s$-wave level spacing for angular momentum $J$. The weak spreading width should be independent of $J$. In practice the average $s$-wave level spacings for the two different spins are not known. We obtained the total $s$-wave level spacing $D_0 = 44.9 \pm 3.1$ eV from the spectroscopy data [17] and assumed that $s$-wave level spacings for the two $J$ values are proportional to $2J+1$.

We assume that the prior probability density function, $P_{\Gamma_w}(\Gamma_w)$, is equal to one up to a value of $\Gamma_{w,max}$, and zero above this value. The likelihood function for a $p$-wave resonance can now be written as

$$L_\mu(\Gamma_w) = P_{\Gamma_w}(\Gamma_w)\left( \sum_{J=0,1} p(J) P_p(p|M_J, A_\mu(J), a, \sigma) + \sum_{J=2} p(J) G(p, \sigma^2) \right). \tag{9}$$

The factor $p(J)$ is the probability that the $p$-wave resonance has total angular momentum $J$, and $M_J$ is the matrix element that corresponds to the weak spreading width $\Gamma_w$. The total likelihood function is the product of the individual likelihood functions for each $p$-wave resonance. The errors on $\Gamma_w$ are given by

$$\ln\left[\frac{L(\Gamma_w^{\pm})}{L(\Gamma_w^*)}\right] = -\frac{1}{2}, \tag{10}$$

where $\Gamma_w^*$ is the most likely value and $\Gamma_w^{\pm}$ gives the confidence range.

The probability that a $p$-wave resonance has angular momentum $J$ is given by the spin distribution, which can be approximated by

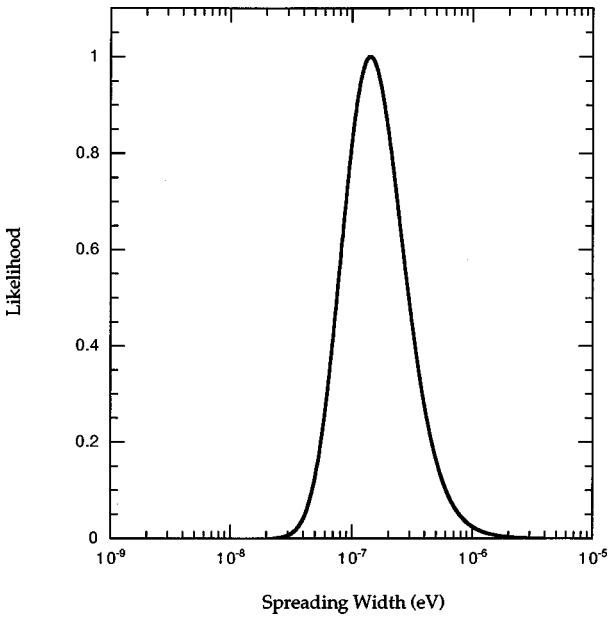


FIG. 4. The likelihood function calculated from the asymmetry data in $^{103}$Rh. The maximum likelihood has been normalized to one.

$$f(J) = \frac{2J+1}{2\sigma_c^2} e^{[-(J+1/2)^2/2\sigma_c^2]}, \tag{11}$$

where $J$ is the total spin, and $\sigma_c$ is the spin cutoff parameter

$$\sigma_c = (0.98 \pm 0.23) A^{(0.29 \pm 0.06)}. \tag{12}$$

The constants in this expression were determined empirically by fitting to nuclei throughout the periodic table [31]. The probability $p(J)$ is found from the normalization $\Sigma_J f(J) = 1$.

All of the low energy (below 500 eV) $s$-wave resonance spins have been determined in previous measurements. Although some of the $s$-wave resonances at higher energies have unknown $J$ values, these resonances have very little effect on the parity violation effects. We verified that the effect of the unknown $s$-wave resonance $J$ values was negligible by detailed calculations, performing the likelihood analysis with the spins of all of these resonances set to $J=0$ and set to $J=1$.

The resulting likelihood curve for $^{103}$Rh is shown in Fig. 4, with a resulting weak spreading width $\Gamma_w = (1.42^{+1.21}_{-0.59}) \times 10^{-7}$ eV.

## V. COMPARISON OF WEAK SPREADING WIDTHS

As discussed in the Introduction, it is of interest to compare the weak spreading width of a mass 100 nucleus with the weak spreading widths determined for $^{232}$Th and $^{238}$U. The weak spreading widths for $^{238}$U and $^{232}$Th are $\Gamma_w = 1.35^{+0.97}_{-0.64} \times 10^{-7}$ eV and $\Gamma_w = 4.7^{+2.7}_{-1.8} \times 10^{-7}$ eV, respectively [9,10].

Our group has recently performed other PNC measurements in the mass 100 region. All weak spreading widths

TABLE II. Summary of weak spreading widths measured by TRIPLE. The mass 100 data have been averaged separately from the mass 230 data. The $\chi^2$ are found by comparing the measured data to the average values in each mass region.

| Target | Reference | $\Gamma_w(10^{-7}$ eV) | $\chi^2$ |
|---|---|---|---|
| $^{93}$Nb | [11] | 0.11[a] | |
| $^{103}$Rh | present | $1.42^{+1.21}_{-0.59}$ | 1.05 |
| $^{107}$Ag | [12] | $2.67^{+2.65}_{-1.21}$ | 0.03 |
| $^{109}$Ag | [12] | $1.30^{+2.49}_{-0.74}$ | 0.50 |
| $^{113}$Cd | [13] | $16.2^{+17.7}_{-8.3}$ | 6.41 |
| $^{121}$Sb[b] | [15] | $6.45^{+9.70}_{-3.70}$ | 1.09 |
| $^{123}$Sb[b] | [15] | $1.23^{+15.0}_{-0.96}$ | 0.13 |
| $^{127}$I[b] | [15] | $2.05^{+1.94}_{-0.93}$ | 0.12 |
| $^{133}$Cs | [16] | $0.006^{+0.16}_{-0.003}$ | 9.11 |
| | Local ave$=2.56^{+0.83}_{-0.63}$ | $\chi^2_{red}=2.63$ | |
| $^{232}$Th | [10] | $4.7^{+2.7}_{-1.8}$ | 1.05 |
| $^{238}$U | [9] | $1.35^{+1.0}_{-0.6}$ | 1.68 |
| | Local ave$=2.90^{+1.30}_{-0.90}$ | $\chi^2_{red}=2.73$ | |
| | Total ave$=2.69^{+0.67}_{-0.54}$ | $\chi^2_{red}=2.13$ | |

[a]The upper limit at 68% confidence limit.
[b]Preliminary results.

published at the present moment by TRIPLE are presented in Table II. In order to compare values for the weak spreading widths, it is useful to note that the likelihood distributions for the weak spreading widths are close to normal when displayed on a log scale. This is illustrated in Fig. 4. Since the curve can be approximated with a Gaussian, the measured values and their uncertainties can be approximated as Gaussian random variables. The weighted averages for the weak spreading widths near mass 100 and 230, and the total weighted average are also listed in Table II. Most of the measured values are within $2\sigma$ of the average value. The value for $^{113}$Cd is anomalously high and the result for $^{133}$Cs is quite low relative to the average spreading width. The upper limit of $0.11\times10^{-7}$ eV (68% confidence level) for $\Gamma_w$ in $^{93}$Nb [11] is also low. This seems to indicate localized fluctuations in the values of $\Gamma_w$, although the overall data are consistent with a constant average value of $\Gamma_w$. However, more data and more analysis are needed to determine definitively both the general mass dependence and whether there are local fluctuations in the spreading width of the effective weak interaction in compound nuclei.

## VI. SUMMARY

The longitudinal asymmetries of neutron $p$-wave cross sections were measured for 32 resonances in $^{103}$Rh in the neutron energy region from 30 to 490 eV. Analysis of these asymmetries was performed using the neutron resonance parameters determined by TRIPLE recently [17]. Statistically significant parity violating asymmetries were observed in the neutron resonances at 44.5, 110.8, 321.6, and 432.9 eV. All measured asymmetries for $p$-waves resonances observed below 490 eV were used in a likelihood analysis to find the weak spreading width. The obtained value $\Gamma_w=1.64^{+1.21}_{-0.59}\times10^{-7}$ eV is consistent with the average value of the weak spreading width in this mass region.

## ACKNOWLEDGMENTS

This work was supported in part by the U.S. Department of Energy, Office of High Energy and Nuclear Physics, under Grant Nos. DE-FG02-97-ER41042 and DE-FG02-97-ER41033, and by the U.S. Department of Energy, Office of Energy Research, under Contract No. W-7405-ENG-36.

[1] E. G. Adelberger and W. C. Haxton, Annu. Rev. Nucl. Part. Sci. **35**, 501 (1998).
[2] V. P. Alfimenkov, S. B. Borzakov, Vo Van Thuan, Yu. D. Mareev, L. B. Pikelner, A. S. Khrykin, and E. I. Sharapov, Nucl. Phys. **A398**, 93 (1983).
[3] J. D. Bowman, G. T. Garvey, Mikkel B. Johnson, and G. E. Mitchell, Annu. Rev. Nucl. Part. Sci. **43**, 829 (1993).
[4] V. V. Flambaum and G. F. Gribakin, Prog. Part. Nucl. Phys. **35**, 423 (1995).
[5] G. E. Mitchell, J. D. Bowman, and H. A. Weidenmüller, Rev. Mod. Phys. **71**, 435 (1999).
[6] O. Sushkov and V. V. Flambaum, JETP Lett. **32**, 352 (1980).
[7] J. D. Bowman *et al.*, Phys. Rev. Lett. **65**, 1192 (1990).
[8] C. M. Frankle *et al.*, Phys. Rev. Lett. **67**, 564 (1991).
[9] B. E. Crawford *et al.*, Phys. Rev. C **58**, 1225 (1998).
[10] S. L. Stephenson *et al.*, Phys. Rev. C **58**, 1236 (1998).
[11] E. I. Sharapov *et al.*, Phys. Rev. C **59**, 1131 (1999).
[12] L. Y. Lowie *et al.*, Phys. Rev. C **59**, 1119 (1999).
[13] S. J. Seestrom *et al.*, Phys. Rev. C **58**, 2977 (1998).
[14] D. A. Smith *et al.*, Bull. Am. Phys. Soc. **42**, 1071 (1997).
[15] Y. Matsuda, Ph.D. thesis, Kyoto University Report No. KUNS 1492, 1998.
[16] E. I. Sharapov *et al.*, Phys. Rev. C **59**, 1772 (1999).
[17] D. A. Smith *et al.*, Phys. Rev. C **60**, 045502 (1999), preceding paper.
[18] P. W. Lisowski, C. D. Bowman, G. J. Russell, and S. A. Wender, Nucl. Sci. Eng. **106**, 208 (1990).
[19] C. M. Frankle, J. D. Bowman, S. J. Seestrom, N. R. Roberson, and E. I. Sharapov, in *Time Reversal Invariance and Parity Violation in Neutron Resonances*, edited by C. R. Gould, J. D. Bowman, and Yu. P. Popov (World Scientific, Singapore, 1994), p. 204.
[20] S. J. Seestrom *et al.*, Nucl. Instrum. Methods Phys. Res. A (to be published).
[21] J. J. Szymanski *et al.*, Nucl. Instrum. Methods Phys. Res. A **340**, 564 (1994).
[22] S. I. Penttila, J. D. Bowman, P. P. J. Delheij, C. M. Frankle, D. G. Haase, R. Mortensen, H. Postma, S. J. Seestrom, and Yi-Fen Yen, in *Time Reversal Invariance and Parity Violation in Neutron Resonances*, edited by C. R. Gould, J. D. Bowman, and Yu. P. Popov (World Scientific, Singapore, 1994), p. 198.
[23] S. I. Penttila, J. D. Bowman, P. P. J. Delheij, C. M. Frankle, D. G. Haase, H. Postma, S. J. Seestrom, and Yi-Fen Yen, in *High*

*Energy Spin Nuclear Physics*, edited by K. J. Heller and S. L. Smith (American Institute of Physics, New York, 1995), p. 532.
[24] J. D. Bowman, S. I. Penttila, and W. B. Tippens, Nucl. Instrum. Methods Phys. Res. A **369**, 195 (1996).
[25] B. E. Crawford *et al.*, in *IV International Seminar on Interaction of Neutrons with Nuclei*, JINR Report No. E3-96-336 (Joint Institute for Nuclear Research, Dubna, 1996), p. 268.
[26] V. W. Yuan *et al.*, Phys. Rev. C **44**, 2187 (1991).
[27] J. D. Bowmam, Y. Matsuda, Y.-F. Yen, and B. E. Crawford (unpublished).
[28] B. E. Crawford, Ph.D. thesis, Duke University, 1998.
[29] J. D. Bowman, L. Y. Lowie, G. E. Mitchell, E. I. Sharapov, and Yi-Fen Yen, Phys. Rev. C **53**, 285 (1996).
[30] A. B. Popov and G. S. Samosvat, Sov. J. Nucl. Phys. **45**, 944 (1987).
[31] T. von Egidy, H. H. Schmidt, and A. N. Behkami, Nucl. Phys. **A451**, 189 (1998).